



Revision of recluse spiders (Araneae: Sicariidae: *Loxosceles*) preserved in Dominican amber and a total-evidence phylogeny of Scytodoidea reveal the first fossil Drymusidae

Ivan L. F. Magalhaes¹, Abel Pérez-González¹, Facundo M. Labarque², Martín Carboni¹, Jörg U. Hammel³, Robin Kunz⁴, Martín J. Ramírez¹, Mónica M. Solórzano-Kraemer⁴

¹ Museo Argentino de Ciencias Naturales “Bernardino Rivadavia”, Consejo Nacional de Investigaciones Científicas y Técnicas (CONICET), Av. Ángel Gallardo 470, C1405DJR, Buenos Aires, Argentina

² Departamento de Ecologia e Biologia Evolutiva (DEBE), Universidade Federal de São Carlos (UFSCar), campus São Carlos, Rodovia Washington Luís, Km 235, CEP 13565-905, São Carlos, SP, Brazil

³ Institute of Materials Physics, Helmholtz-Zentrum Hereon, Outstation at DESY, Max-Planck-Str. 1, D-21502 Geesthacht, Germany

⁴ Department of Palaeontology and Historical Geology, Senckenberg Research Institute and Natural History Museum, D-60325 Frankfurt am Main, Germany

<http://zoobank.org/References/09338026-092F-42FB-8E2F-00DD6B868D49>

Corresponding author: Ivan L. F. Magalhaes (magalhaes@macn.gov.ar)

Received 29 April 2022

Accepted 10 August 2022

Published 28 September 2022

Academic Editors Lorenzo Prendini, Klaus-Dieter Klass

Citation: Magalhaes ILF, Pérez-González A, Labarque FM, Carboni M, Hammel JU, Kunz R, Ramírez MJ, Solórzano-Kraemer MM (2022) Revision of recluse spiders (Araneae: Sicariidae: *Loxosceles*) preserved in Dominican amber and a total-evidence phylogeny of Scytodoidea reveal the first fossil Drymusidae. Arthropod Systematics & Phylogeny 80: 541–559. <https://doi.org/10.3897/asp.80.e86008>

Abstract

Recluse or violin spiders in the genus *Loxosceles* (Scytodoidea: Sicariidae) are a diverse group (~140 extant species) including medically important species and distributed mainly in the Americas, Africa, and the Mediterranean region. In addition, this genus includes three fossil species from Miocene Dominican amber. Here we revise the taxonomy of these fossil species by examining, imaging and re-describing their type specimens. We find that *L. defecta* Wunderlich, 1988 and *L. deformis* Wunderlich, 1988 are *bona fide* members of the genus and report additional characters overlooked in their original descriptions. We further study the holotype of *L. aculicaput* Wunderlich, 2004 using synchrotron radiation micro-computed tomography to reveal previously unknown morphological details hidden by fissures in the amber. We found several characters inconsistent with *Loxosceles* but consistent with *Drymusa* (false violin spiders; Scytodoidea: Drymusidae), such as three claws, well-developed podotarsite, and a broad colulus. This suggests the species is misplaced in *Loxosceles*. To test this hypothesis, we estimated a total-evidence phylogeny of the superfamily Scytodoidea including extant and fossil taxa, morphological data, traditional molecular markers, and sequences of ultra-conserved elements. The results show unambiguously that *L. aculicaput* belongs to *Drymusa* and is a close relative of extant species of the genus inhabiting the Greater Antilles. Therefore, we here transfer this species to *Drymusa*, establishing a new combination and new family assignment. *Drymusa aculicaput* **comb. nov.** represents the first known fossil Drymusidae and shows that crown members of this genus already existed in the Miocene.

Keywords

Drymusa, micro-CT, UCE, Miocene

1. Introduction

Spiders are a speciose clade of predators containing ~50000 species (WSC 2022), which play a key role in terrestrial food webs (Nyfeller and Birkhofer 2017). Despite their diversity, abundance, and ubiquity, they have delicate bodies, and thus, they only fossilize in exceptional conditions (Selden and Penney 2010). In fact, over three-quarters of the ~1400 species of fossil spiders are preserved as inclusions in amber coming principally from three deposits in northern Myanmar (Late Cretaceous), the Baltic Sea (Eocene), and the Dominican Republic (Miocene) (Dunlop et al. 2020; Magalhaes et al. 2020). While it has been shown that arthropods entrapped in natural resins are only a subset of the total community present in the environment (Solórzano Kraemer et al. 2018), fossils preserved in amber provide an important glimpse into the past diversity of spiders.

Miocene amber from the Dominican Republic is the major source of spider fossils in the Neotropical region. Around 170 currently valid species have been named from this deposit (Dunlop et al. 2020), most of them (~120) described in the monographic treatment of this fauna by Wunderlich (1988) (for a historical account on the taxonomy of fossil spiders from Dominican amber see Selden and Penney 2010: 181). Penney and Pérez-Gelabert (2002) compared the fossil fauna with the composition of extant Hispaniolan spiders. While a poor knowledge of extant spiders hampers a more detailed comparison, they showed that many families and genera are shared between the faunas, showing that the deposit represents a typical tropical assemblage. Interestingly, some families and genera are known from the islands only from fossils, prompting the hypothesis that extant members might be present in Hispaniola but remain undiscovered (Penney 1999). This is certainly more probable for specimens described in Holocene copal or Defaunation resin from the Dominican Republic (e.g., Wunderlich 1986) since these resins can have an age of only 60 years BP (conventional radiocarbon age) (Solórzano-Kraemer et al. 2020). For some families, this hypothesis has been confirmed, such as for Filistatidae, initially known from Hispaniola by fossil specimens (Penney 2005) but later showed to include extant Dominican taxa endemic to the island (Brescovit et al. 2016). Some families with extant Hispaniolan taxa have hitherto not been recorded in amber, such as Drymusidae, which includes *Drymusa simoni* Bryant, 1948 from Haiti (see WSC 2022) and unidentified species from the Dominican Republic (Solánlylly Carrero, pers. comm.). This spider family has so far no fossil record at all (Dunlop et al. 2020).

Dominican amber yields the only fossils known for a few spider families, such as Sicariidae. Sicariids include six-eyed sand spiders (*Sicarius* Walckenaer, 1847 and *Hexophthalma* Karsch, 1879) and recluse or violin spiders (*Loxosceles* Heineken et Lowe, 1832). The family belongs to Synspermiata, a major spider clade that is well-represented in Cretaceous amber (Magalhaes et al. 2020), and molecular clocks estimate that sicariid genera originated in the Cretaceous (Binford et al. 2008;

Magalhaes et al. 2019). Despite that, the family has only three known fossils preserved in middle Miocene Dominican amber: *Loxosceles defecta* Wunderlich, 1988, *L. deformis* Wunderlich, 1988 and *L. aculicaput* Wunderlich, 2004. Violin spiders comprise ~140 described species distributed mainly in the Americas, Africa, and the Mediterranean region (WSC 2022), ranking among the most speciose spider genera. They are infamous because of their medical importance (Vetter 2008), but are also important models for biogeography (e.g., Binford et al. 2008; Planas and Ribera 2014). A better knowledge of the three *Loxosceles* fossil species would be desirable since they provide the only suitable calibration point for estimating the dated phylogenetic trees of this family. Because they are only known from their original descriptions (Wunderlich 1988, 2004), we here strive to revise their morphology and taxonomy.

During a preliminary examination of the holotype of *L. aculicaput*, we found that some of its characters are inconsistent with a placement in *Loxosceles*, such as the presence of three tarsal claws and a well-delimited podotarsite (the genus has only two tarsal claws and a poorly delimited podotarsite; see Labarque and Ramírez 2012). These observations suggested that this species was misplaced in *Loxosceles*. Unfortunately, the holotype is preserved in a piece of amber with large fissures that prevent a clear examination of its ventral side, including the palps, the morphology of which has a high taxonomic value. Recently, the use of X-ray micro-computed tomography (μ -CT) and synchrotron radiation micro-computed tomography (SR μ -CT) has been employed to enhance taxonomic descriptions of fossils (e.g., Penney et al. 2007, 2012; Saupé et al. 2012) and to reveal morphological details hidden in the piece, or even in completely opaque amber, allowing a better assessment of the systematic placement of the fossil (e.g., Soriano et al. 2010; Dunlop et al. 2011; Azevedo et al. 2021; Solórzano Kraemer et al. 2011, 2015, 2022). Thus, the use of this technique might help shed light on the phylogenetic placement of *L. aculicaput*.

Recently, systematic advances in spiders have relied heavily upon genomic-scale molecular data (e.g., Kulkarni et al. 2020; Ramírez 2021). While this approach has proved to be a powerful tool for resolving recalcitrant relationships, most of these studies include only molecular data in their phylogenetic matrices. There are legacy morphological matrices that may be used alongside the newly collected molecular data (e.g., Griswold et al. 2005; Labarque and Ramírez 2012; Ramírez 2014). This total evidence approach is useful in testing the placement of taxa for which molecular data is unavailable, such as fossils (e.g., Wood et al. 2013; Wood 2017; Mongiardino Koch et al. 2021; Azevedo et al. 2021; Magalhaes and Ramírez 2022). We thus expect that a phylogenetic analysis including molecular and morphological data is the most straightforward way to test the phylogenetic relationships between the fossils treated here and the extant members of Scytodoidea.

The aims of this contribution are: (1) to revise the taxonomy of Dominican amber *Loxosceles*, re-illustrate the

type specimens and re-assess their morphology; and (2) to test the phylogenetic placement of the fossils using a dataset containing morphological and sequence data for representatives of all extant Scytodoidea families.

2. Material and Methods

2.1. Specimens and collections

Examined specimens, fossil or extant, are housed in the following collections (curators in parentheses): IBSP – Instituto Butantan, São Paulo, Brazil (A. D. Brescovit); MACN-Ar – División Aracnología, Museo Argentino de Ciencias Naturales “Bernardino Rivadavia”, Buenos Aires, Argentina (M. J. Ramírez); MCZ – Museum of Comparative Zoology, Harvard, USA (G. Giribet and M. Srivastava); MNHNCu – Museo Nacional de Historia Natural de Cuba, Havana, Cuba (G. Alayón García); SMF-Be – Amber Collection, Senckenberg Research Institute and Natural History Museum, Frankfurt, Germany (M. M. Solórzano-Kraemer), SMNG – Senckenberg Museum für Naturkunde Görlitz, Görlitz, Germany (A. Christian).

Amber pieces were re-polished at the SMF using a Phonix Beta polishing machine with grinding paper for metallography, wet and dry: Grip 2500 and 4000. After polishing, pieces were embedded in Araldite 2020® Epoxy resin following Sadowski et al.’s (2021) recommendations.

2.2. Extant material examined for comparison

The following specimens have been examined for the new scorings of the morphological matrix, or to discuss the morphology of scytodoids. We scored *Ochyrocera diablo* Pérez-González, Rubio et Ramírez, 2016 using the data from the original description (Pérez-González et al. 2016).

Altheopus maechamensis Li et Li, 2018 (Psilodercidae): THAILAND • 1 ♂ 1 ♀; Chiang Mai, Doi Inthanon National Park; 18.53°N 98.5025°E; 6 Oct 2003; ATOL Expedition 2003 leg.; MACN-Ar 35342.

Drymusa spectata Alayón, 1981 (Drymusidae): CUBA • 1 ♂ 1 immature; Cienfuegos; Comanaqua (Cumanayagua); cueva del Canto; 750 m a.s.l.; 21.8930°N 80.1486°W; 20 August 2002; J. M. Ramos leg.; MNHNCu.

Drymusa armasi Alayón, 1981 (Drymusidae): CUBA • 1 ♂ 1 ♀; Santiago de Cuba, Gran Piedra; under rocks; 1100 m a.s.l.; 20.083333°N 75.623611°W; 21 June 1982; L. F. Armas leg.; MNHNCu.

Drymusa simoni Bryant, 1948 (Drymusidae): HAITI • 1 ♂ (holotype) 1 ♀; Nord-Ouest, LaHotte; 16–17 Oct 1934; P. J. Darlington leg.; MCZ 23101. 2 immatures; same data as the holotype; MCZ 44196.

Loxosceles caribbaea Gertsch, 1958 (Sicariidae): CUBA • 2 ♂ 4 ♀; Santiago de Cuba, Reserva Ecológica Siboney-Jutici, Cueva La Vir-

gen; 19.96083°N 75.7144°W; 04 May 2010; A. Pérez González leg.; MACN-Ar 32734, MACN-Ar 32736.

Loxosceles cubana Gertsch, 1958 (Sicariidae): CUBA • 2 ♂ 2 ♀; Pinar del Río; Viñales; Cueva del Cable; 22.6677°N 83.7094°W; A. Sánchez leg.; 20 April 2012; IBSP 164702.

Loxosceles deserta Gertsch, 1973 (Sicariidae): USA • 1 ♂ 1 ♀; Arizona, Tucson; F. E. Russell leg.; MACN-Ar 21497, MACN-Ar 21498.

Loxosceles hirsuta Mello-Leitão, 1931 (Sicariidae): ARGENTINA • 1 ♂; San Luis, Junín, Establecimiento La Clotilde; 32.19955°S 65.59549°W; 10 January 2017; M. Ramírez et J. Faivovich leg.; MACN-Ar 38707.

Loxosceles laeta (Nicolet, 1849) (Sicariidae): BRAZIL • 3 ♂ 3 ♀; São Paulo, Osasco; 23.5325°S 46.7916°W; 26 Jul. 1982; J. R. Bettinazzi leg.; IBSP 34948.

Loxosceles rufescens (Dufour, 1820) (Sicariidae): ISRAEL • 1 ♂ 1 ♀; HaZafon, near Elon, Nahal Bezet Nature Reserve; 33.0740°N 35.2379°E; 17 February 2020; I. L. F. Magalhaes, E. Gavish-Reguev, Z. Ganem, S. Aharon, N. Givon et M. Arnedo leg.; MACN-Ar 41223.

Loxosceles simillima Lawrence, 1927 (Sicariidae): NAMIBIA • 2 ♂ 2 ♀; Waterberg; 20.352701°S 17.337579°E; M. Stockmann leg.; MACN-Ar 39459.

Loxosceles taino Gertsch et Ennik, 1983 (Sicariidae): DOMINICAN REPUBLIC • 1 ♂ 2 ♀; Pedernales; no collecting date; A. Sánchez leg.; IBSP 164710.

2.3. Light microscopy

The photographs and Z-stacks images of fossil species were taken under a Nikon SMZ25 microscope, using Nikon SHR Plan Apo 0.5× and SHR Plan Apo 2× objectives with a microscope camera Nikon DS-Ri2 and the NIS-Element software (version 4.51.00; www.microscope.healthcare.nikon.com). In some cases, to prevent diffraction caused by irregular surfaces of the amber piece, we placed a coverslip and a drop of water with sugar on top of the piece to flatten the surface to be photographed.

Morphological observations on extant specimens were made using Leica M165 C and Leica M125 stereomicroscopes. Pictures were taken with Nikon DXM1200 digital camera mounted on a stereoscopic microscope Nikon SMZ1500 and on a microscope Leica DM4000 M, and with a Leica DFC 500 digital camera mounted on a stereoscopic microscope Leica M165 C or Leica M216. Extended focal range images were composed with the Leica Application Suite version 3.6.0. or Helicon Focus 3.10.3–4.62 (<https://www.heliconsoft.com>, Ukraine). Preparations were carefully cleaned using fine brushes and a thin jet of alcohol from a thinned pipette; some setae were removed to expose structures, especially those on legs, palps, spinnerets, and chelicerae.

2.4. Scanning electron microscopy

For scanning electron microscope (SEM), all preparations were dehydrated in a series of increasing concentrations of ethanol (80%, 90%, 95%, 100%), and critical-point dried. After drying and brushing, they were mounted on

adhesive copper tape (Electron Microscopy Sciences, EMS 77802) affixed to a stub and secured with a conductive paint of colloidal graphite on isopropyl alcohol base (EMS 12660). Prior to SEM examination under a high vacuum with a FEI XL30 TMP or a LEO 1450VP, the structures were sputter-coated with Au-Pd.

2.5. Synchrotron radiation micro-computed tomography

The imaging of the holotype of *L. aculicaput* was performed at the Imaging Beamline – IBL P05 - PETRA III at Deutsches Elektronen Synchrotron (DESY) in Hamburg, operated by the Helmholtz-Zentrum Hereon (Greving et al. 2014; Wilde et al. 2016). The specimen was imaged at a photon energy of 18 keV using a commercial CMOS camera system with an effective pixel size of 1.28 μm . The sample to detector distance was set to 3 cm. For each tomographic scan, 3601 projections at equal intervals between 0 and π were recorded. Tomographic reconstruction was done by applying transport of intensity phase retrieval approach and using the filtered back-projection algorithm (FBP) implemented in a custom reconstruction pipeline (Moosmann et al. 2014) using Matlab (MathWorks) and the Astra Toolbox (Palenstijn et al. 2011; van Aarle et al. 2015; van Aarle et al. 2016). For processing, raw projections were binned two times, resulting in an effective pixel size of the reconstructed volume of 2.56. The complete specimen was segmented in three dimensions using region-growing techniques in VGStudioMax (version 3.3.1 www.volumegraphics.com/de, Volume Graphics, Heidelberg, Germany).

We carried out the segmentation and volume rendering of the pedipalps in AMIRA5.4.5 (FEI Visualization Science Group, Burlington, MA, USA). All images were post-processed to adjust contrast and sharpness using Photoshop CS6 (Adobe Inc., San Jose, CA, USA).

2.6. Phylogenetic analyses

We augmented the morphological matrix of Scytodoidea families (Labarque and Ramírez 2012) by including the following taxa: *Ochyrocera diablo*, *Altheopus maechamensis*, *Loxosceles defecta*, and *L. aculicaput*. We added the first two to include all extant Scytodoidea families in the sampling, and the latter two to test their phylogenetic position. *Loxosceles deformis* was not included because the only known specimen is poorly preserved and most characters needed in the matrix are not observable.

We added the following characters to accommodate the morphological diversity brought by newly incorporated taxa:

- (102) Chelicerae promarginal lobe, shape: (0) small and rounded, (1) large and detached, (2) with a distal prolongation (Fig. 7C).
 (103) Chelicerae medial lamina, apex shape: (0) simple, (1) bifid (Fig. 1D).

- (104) Colulus, shape: (0) lobe-like, (1) broad, plate-like (Fig. 7I).
 (105) Male, leg I, femur, prolateral macrosetae: (0) absent, (1) present (Fig. 3C).
 (106) Labium, apex, shape: (0) straight, (1) pointed, (2) notched (Fig. 7B).
 (107) Podotarsite, divisions: (0) single unit, (1) subdivided by additional articulation (see Labarque et al. 2017 for explanations of characters 107–109).
 (108) Podotarsite, cuticle on dorsal side: (0) membranous, open podotarsite; (1) sclerotized, closed podotarsite.
 (109) Podotarsite, distal dorsal hood: (0) absent, (1) present.
 (110) Chelicerae, promarginal lobe, distal prolongation, shape: (0) curved, rounded; (1) straight, pointed (Fig. 7C).

We added legacy genetic data from six target-gene markers from the mitochondrial (12S rRNA, 16S rRNA, COI) and nuclear (histone H3, 18S rRNA, 28S rRNA) genomes, and genomic ultra-conserved elements (Table 1). To maximize morphological and genetic data overlap, we merged data from closely related species into a single terminal in the outgroup genera *Stedocys*, *Ariadna*, *Altheopus*, and *Ochyrocera* (Table 1). The alignment of target-gene markers was made with the online version of MAFFT (Katoh et al. 2019) with the L-INS-I option, which resulted in a total length of 6458 sites (12S 333 sites; 16S 469; 18S 1746; 28S 2348; COI 1235; H3 327).

Published UCE and transcriptome sequences were downloaded from the Sequence Read Archives using fastq-dump v. 2.11 (SRA Toolkit Development Team: <https://hpc.nih.gov/apps/sratoolkit.html>) with the flags `-gzip -clip -split-files -qual-filter` to remove adapters and trim low-quality base calls. Sequence reads were trimmed using TRIMMOMATIC v. 0.39 (Bolger et al. 2014), with parameters LEADING:20 TRAILING:20 SLIDINGWINDOW:4:20 MINLEN:30 HEADCROP:5 and `-phred 33`, and assembled using SPAdes genome assembler v3.15.3 (Prjibelski et al. 2020) with parameters single-cell flag and coverage cutoff value auto. Duplicates were removed using CD-HIT version 4.8.1 (Fu et al. 2021) with parameters: sequence identity threshold 0.95, word_length 10. The sequences were processed with the PHYLUCE v. 1.7.1 (Faircloth 2016) pipeline. We matched the assembled sequences to a compilation of UCE probes merging the Arachnid probe set (Starrett et al. 2017), and the Spider probe set (Kulkarni et al. 2020). Sequences were aligned using MAFFT v. 7.455 and trimmed with GBLOCKS v. 0.31b (Castresana 2000), with the default parameters implemented in PHYLUCE. The recovery of UCE markers did not work well with the few taxa represented in our analysis, probably because few markers were shared by several species; this small dataset failed to recover the monophyly of well-established groups, such as the genus *Loxosceles*. We then used a wider sample of 100 short-read archives from 75 species of Synspermiata and outgroups (Table 1), which recovered 1912 markers with a minimum coverage of 10%, and a total length of 510,125 sites. From this data-

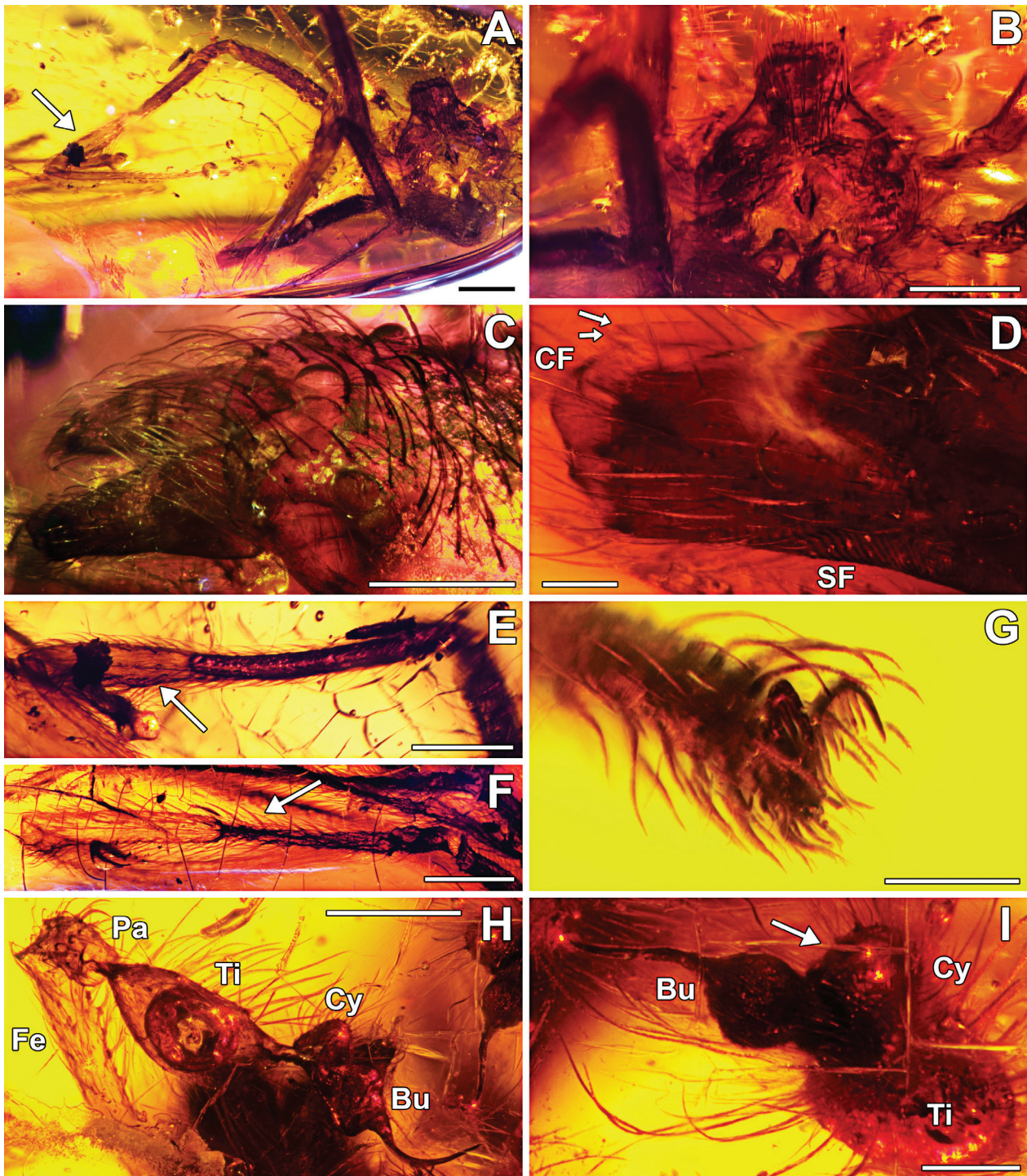


Figure 1. *Loxosceles defecta* Wunderlich, 1988, holotype (SMF-Be 970a; A, B, E, G–I) and paratype (SMF-Be 970b; C, D, F) embedded in the same amber piece, photographs under light microscopy. **A** habitus, dorsal view. Arrow to incrassate tibia I. **B** prosoma, dorsal view. **C** prosoma, subanterior view. Note six eyes in three dyads. **D** left chelicera, subanterior view. Arrows to bifid apex of cheliceral lamina. **E** left tibia I, retrolateral view. Arrow to incrassate region with strong macrosetae. **F** right tibia I, dorsal view. Arrow to strong macrosetae. **G** left tarsus I, apical view. Note absence of third claw. **H** right palp, retrolateral. **I**: left bulb, dorsal. Arrow to prolateral lobe of the cymbium. Scale bars: 1 mm (A, B, E, F), 0.5 mm (C, H), 0.2 mm (I) 0.1 mm (D, G).

set, we selected the target species, which were analyzed together with the target-gene markers and morphological data.

The phylogenetic analysis under maximum likelihood was done with IQ-TREE v. 2.1.3 (Minh et al. 2020), selecting models for each target gene and the concatenated UCE markers by Bayesian information criterion with

ModelFinder (Kalyaanamoorthy et al. 2017), and estimating support with 1000 rounds of ultrafast bootstrap (Hoang et al. 2018). The models selected were: UCE GTR+F+I+G4, 12S TIM2+F+G4, 16S TIM2+F+I+G4, 18S TNe+R3, 28S TIM3+F+R3, COI TIM3+F+I+G4, H3 K2P+R2. We removed the invariant characters of the morphological partition and replaced polymorphic scor-

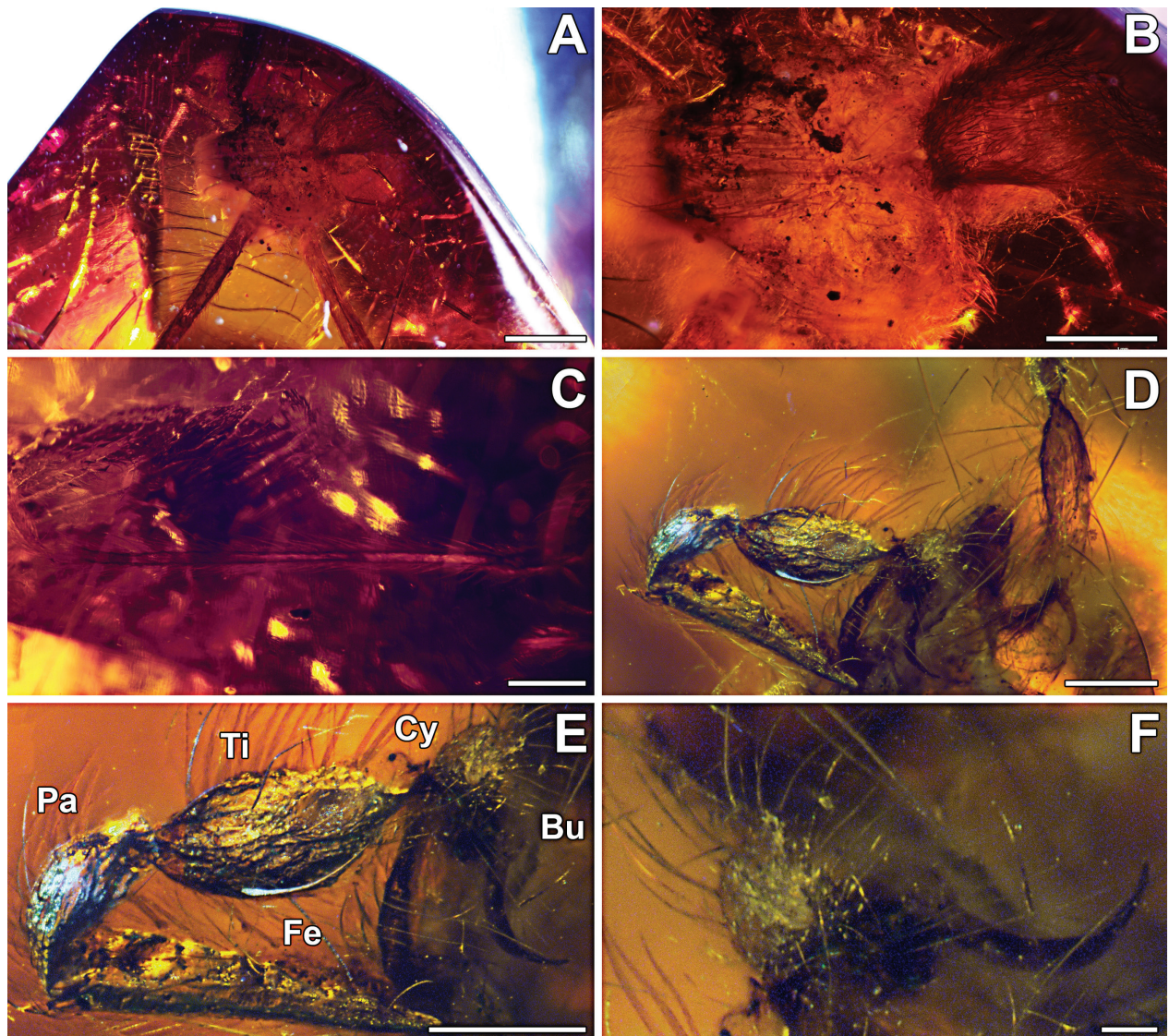


Figure 2. *Loxosceles deformis* Wunderlich, 1988, holotype (SMF-Be 968a), photographs under light microscopy. **A, B** habitus, dorsal view. **C** left tibia I, prolateral. **D** palps, subventral view. **E** right palp, retrolateral view. **F** right bulb, retrolateral view. Scale bars: 2 mm (A), 1 mm (B, C), 0.5 mm (D, E), 0.1 mm (F).

ings with missing entries. Morphological data were analyzed afterwards as two separate partitions, one for 74 unordered characters, treated with the Mk model, and the other for 5 ordered characters, with the Ordered model; both partitions were corrected for the absence of invariant characters with the Asc model. The analysis under maximum parsimony was done with TNT v. 1.5 (Goloboff and Catalano 2016), under equal weights; since 100 out of 100 heuristic searches of 1 RAS followed by TBR branch swapping reached the same tree and length, it is likely that the optimal tree was found. We estimated branch support with 1000 rounds of bootstrap. Synapomorphies were calculated with TNT.

2.7. Abbreviations

ALS = anterior lateral spinneret, Bu = bulb, Ch = chelicera, Co = colulus, Cy = cymbium, CF = cheliceral fang, e = embolus, Fe = femur, Pa = patella, PLS = posteri-

or lateral spinneret, PMS = posterior median spinneret, SF = stridulatory file, Ti = tibia.

2.8. Data resources

The supplementary figures and data underpinning the analyses reported in this paper are deposited in the Zenodo repository at <https://zenodo.org/record/6954956> under [www.doi.org/10.5281/zenodo.6954956](https://doi.org/10.5281/zenodo.6954956).

3. Results

3.1. Imaging results

We present new photographs under light microscopy of the holotypes of *Loxosceles defecta* (Fig. 1), *L. deformis*

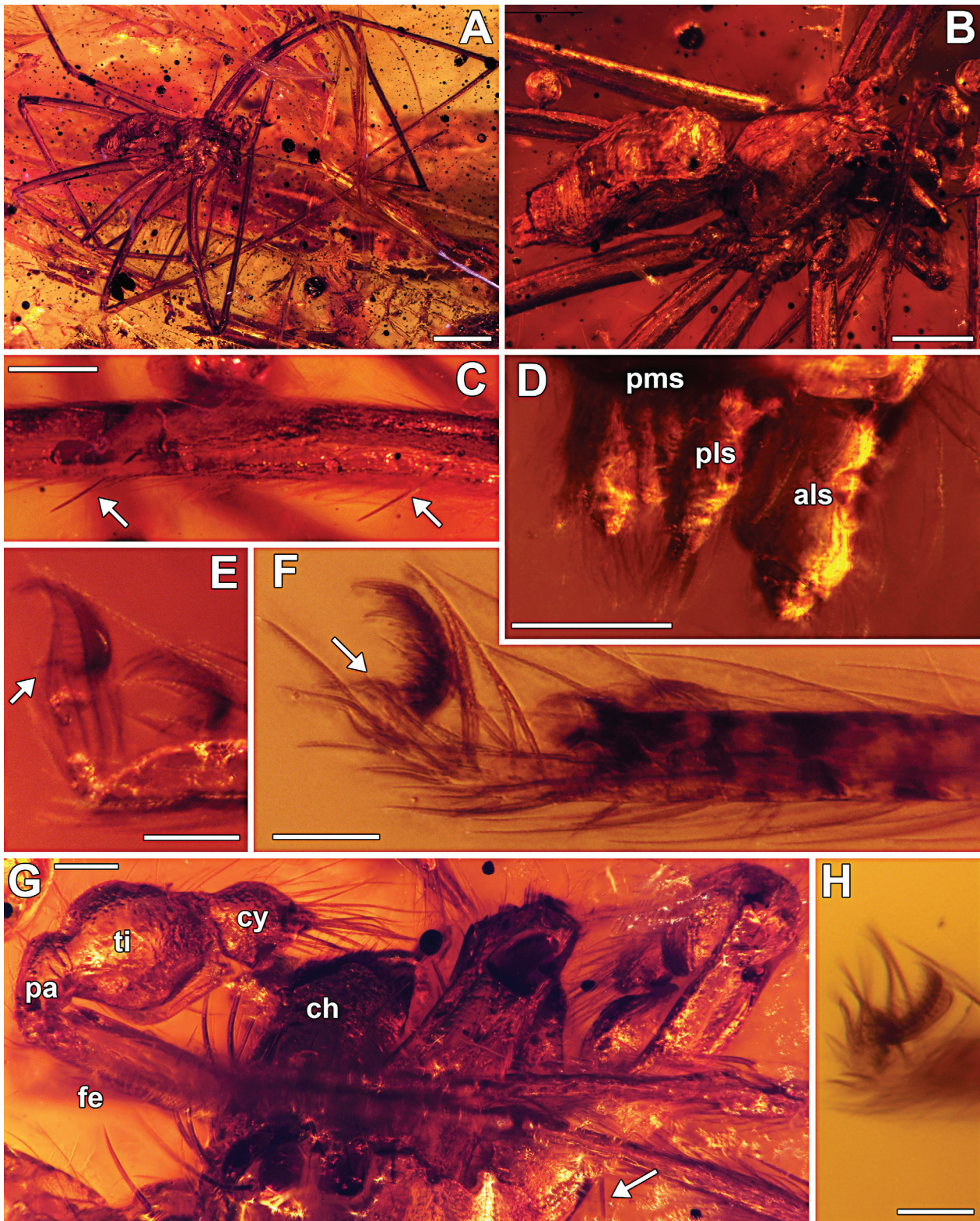


Figure 3. *Drymusa aculicaput* (Wunderlich, 2004) **comb. nov.**, holotype (SMNG 07/36287-422), photographs under light microscopy. **A, B** habitus, dorsolateral. **C** right femur I. Arrows to anterior macrosetae. **D** spinnerets, dorsolateral view. **E, F, H** right tarsi (**E**: III–IV, **F**: II, **H**: I), prolateral. Arrows to third claw. Note highly articulated podotarsite. **G** Chelicerae and palp, subdorsal view. Arrow to tip of right embolus. Scale bars: 1 mm (**A**), 0.5 mm (**B**), 0.2 mm (**C**), 0.1 mm (**D, G**), 0.05 mm (**E, F, H**).

(Fig. 2) and *L. aculicaput* (Fig. 3). This revealed some details that had been overlooked in the original descriptions, such as a third tarsal claw in *L. aculicaput* (Fig. 3E–F), or the modified legs, bifid cheliceral lamina and stridulatory files in the chelicerae of *L. defecta* (Fig. 1D–F).

The phylogenetic significance of these observations is discussed below (see 4.2.). In the case of *L. aculicaput*, a large fissure in the amber prevented observation of the ventral aspects of the specimen, and thus only the dorsal side could be imaged (Fig. 3), hampering a detailed

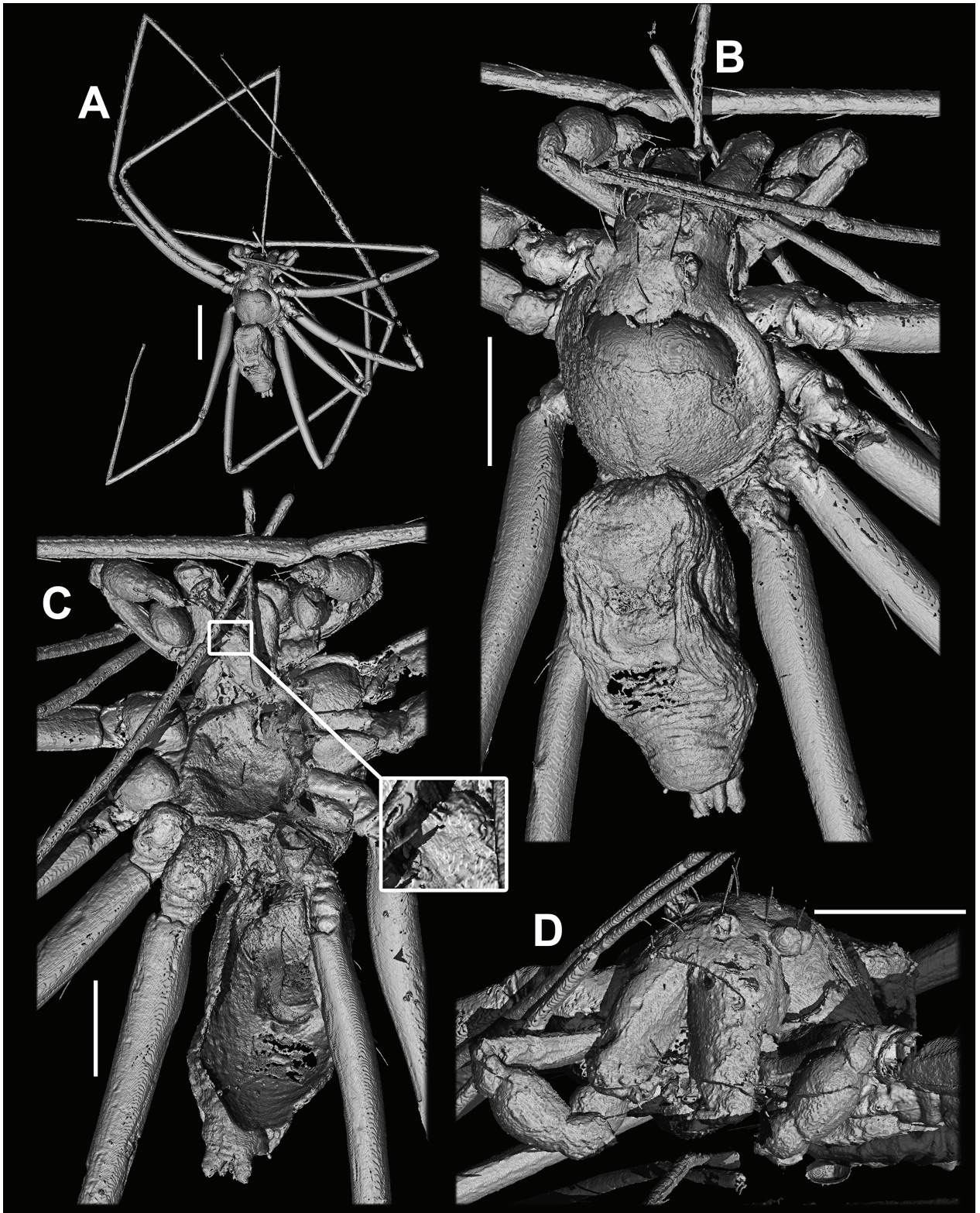


Figure 4. *Drymusa aculicaput* (Wunderlich, 2004) **comb. nov.**, holotype (SMNG 07/36287-422), rendered volume after image stack obtained with synchrotron radiation micro-computed tomography. **A, B** habitus, dorsal. **C** habitus, ventral. Inset showing notched labium. **D** clypeus, subanterior. Scale bars: 1 mm (A), 0.5 mm (B–D).

examination of some taxonomically important structures, such as the palps (Fig. 3G).

After scanning the amber piece containing the holotype of *L. aculicaput*, we rendered a 3D reconstruction of the specimen (Figs 4, 5) that revealed additional details of key ventral structures of the spider, such as a notched

labium (Fig. 4C, inset), a broad colulus (Fig. 5A, B) and the shape of both pedipalps (Fig. 5D–J). It also allowed better visualization of the spinnerets, which are disposed of in a compact group (Fig. 5B); the ALS are about the same length as the PLS (Figs 3D, 5C). The resolution did not resolve some of the smaller structures, such as the

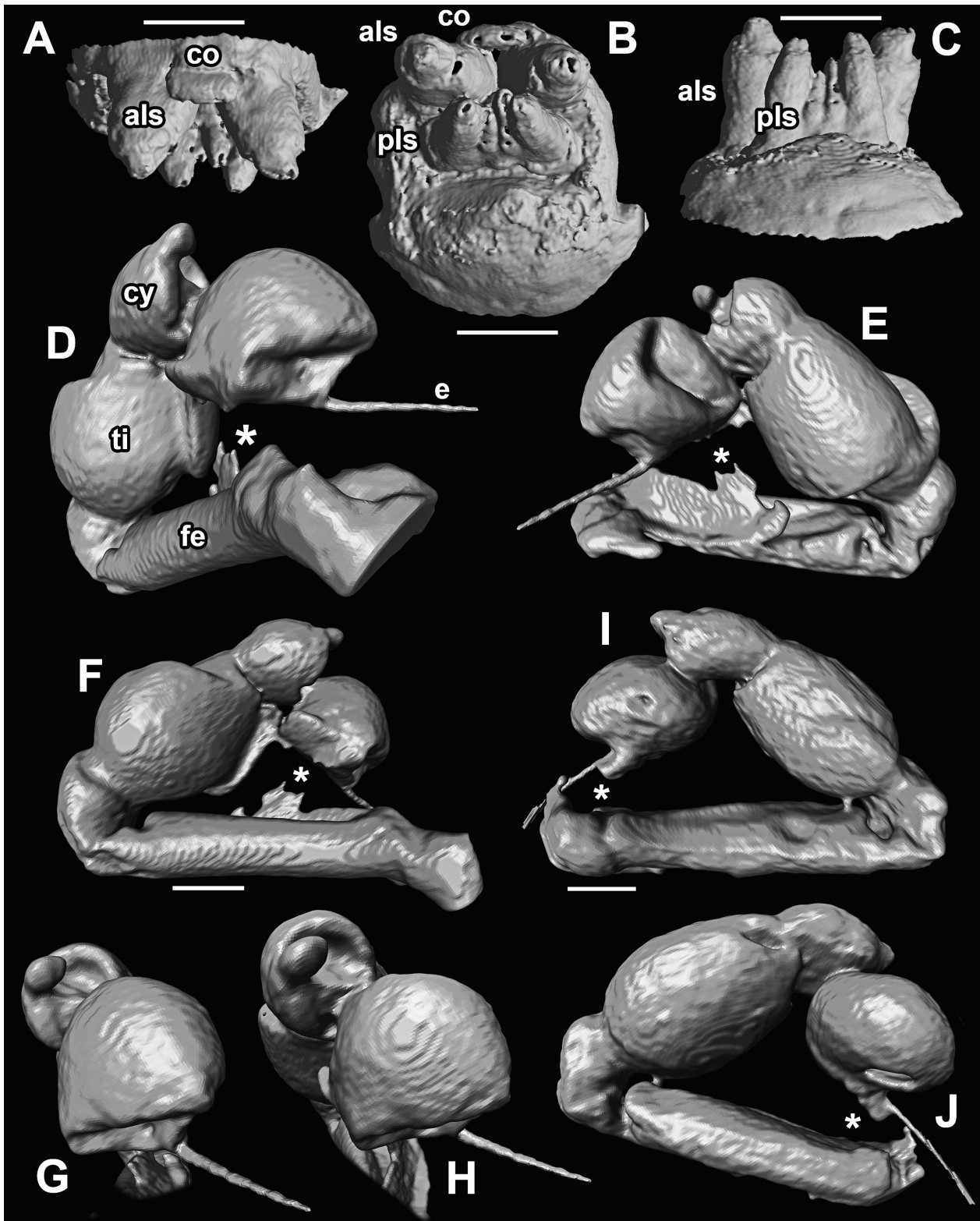


Figure 5. *Drymusia aculicaput* (Wunderlich, 2004) **comb. nov.**, holotype (SMNG 07/36287-422), rendered volume after image stack obtained with synchrotron radiation micro-computed tomography. Spinnerets (A–C), left palp (D–H), and right palp (I, J). A ventral. B apical. C dorsal. D subprolateral. E retrolateral. F prolateral. G bulb and cymbium, apical. H bulb and cymbium, dorsal. I prolateral. J retrolateral. Asterisks are artifacts in the rendering. Scale bars: 0.1 mm (only A–C, F, I to scale).

number of tarsal claws (although these can be seen in Fig. 3E, F), the presence and number of cheliceral teeth, or the presence of a double row of teeth in the first and second prolateral claws of the legs. The 3D rendering of the genitalia shows some aberrant structures (marked with an

asterisk in Fig. 5) that we interpret as artifacts (perhaps thin layers of air surrounding the specimen) since each is only present in a single palp and similar structures are lacking in related species (see Fig. 7).

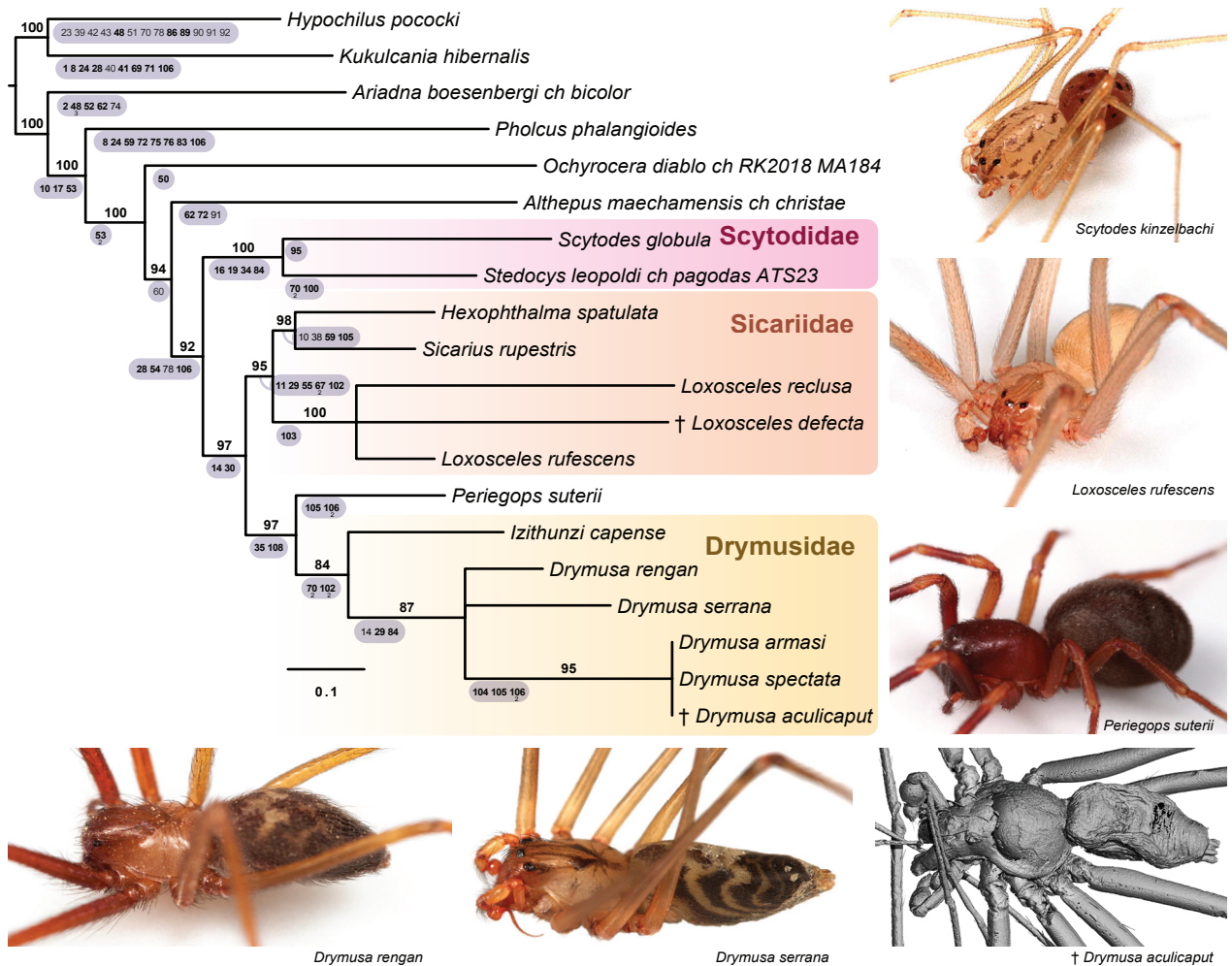


Figure 6. Relationships among Scytodoidea inferred under maximum likelihood using a combined dataset (morphology + target genes + ultraconserved elements). Taxa with “ch” in their names are chimeras formed by combining morphological data of a species with sequence data of a congener. Bootstrap percentages are above branches, apomorphies below branches (state 0 in regular font, state 1 in bold font, states 2–3 indicated below character number).

3.2. Phylogenetic analyses

The target-gene and UCE datasets produced similar trees (Figs S1, S2), with higher support in the last case, as expected. The combination of all sequence data (Fig. S3) produced a tree with all the groups in agreement with the UCE analysis. The morphological dataset produced trees with the same resolution for Sicariidae, Scytodidae, Periegopidae, and Drymusidae, but discordant with the molecular data in the more basal splits, also differing between maximum likelihood (ML) and maximum parsimony (MP) analyses (Fig. S4). The ML and MP analyses of the complete dataset produced very similar results, only differing in three polytomies of the MP tree, that were resolved in the ML tree (Fig. 6; Fig. S5). Because these resolved branches in the ML tree had bootstrap below 75% and no molecular or morphological synapomorphies, we base our subsequent analyses on the phylogeny with those branches collapsed (Fig. 6). The morphological matrix, DNA alignments, and the total evidence tree found under ML are available as Supplementary material 2, 3, and 4, respectively.

The total evidence analysis (Fig. 6) recovered a monophyletic Scytodoidea including Ochyroceratidae, Psilo-

dercidae, and Scytodidae as three successive splits in the base of the superfamily. Sicariidae is recovered including Sicariinae (*Hexophthalma* + *Sicarius*) and two extant species of *Loxosceles* grouped with the fossil *L. defecta*. This family is recovered as sister to Periegopidae + Drymusidae. Within Drymusidae, the South African *Izithunzi* Labarque, Pérez-González and Griswold, 2018 is recovered as the sister group to a clade containing American *Drymusa* Simon, 1892 and *Loxosceles aculicapot*. This latter species is recovered in a clade of Antillean species (*D. armasi* Alayón, 1981 and *D. spectata* Alayón, 1981 from Cuba).

Sicariidae is supported by five unambiguous morphological apomorphies, only one of which is observable in the fossils (third tarsal claw absent; Fig. 1G; Labarque and Ramírez 2012: fig. 8). *Loxosceles* is supported in our tree by a single unambiguous morphological apomorphy (cheliceral lamina with bifid apex; Fig. 1D; Magalhaes et al. 2017a: fig. 14A); two additional potential synapomorphies from spigots, chars. 73-1 and 82-1, were not visible in the fossil species. Drymusidae is supported by the promarginal lobe of the chelicerae with a distal prolongation (Labarque et al. 2018: fig. 3D), and the presence of

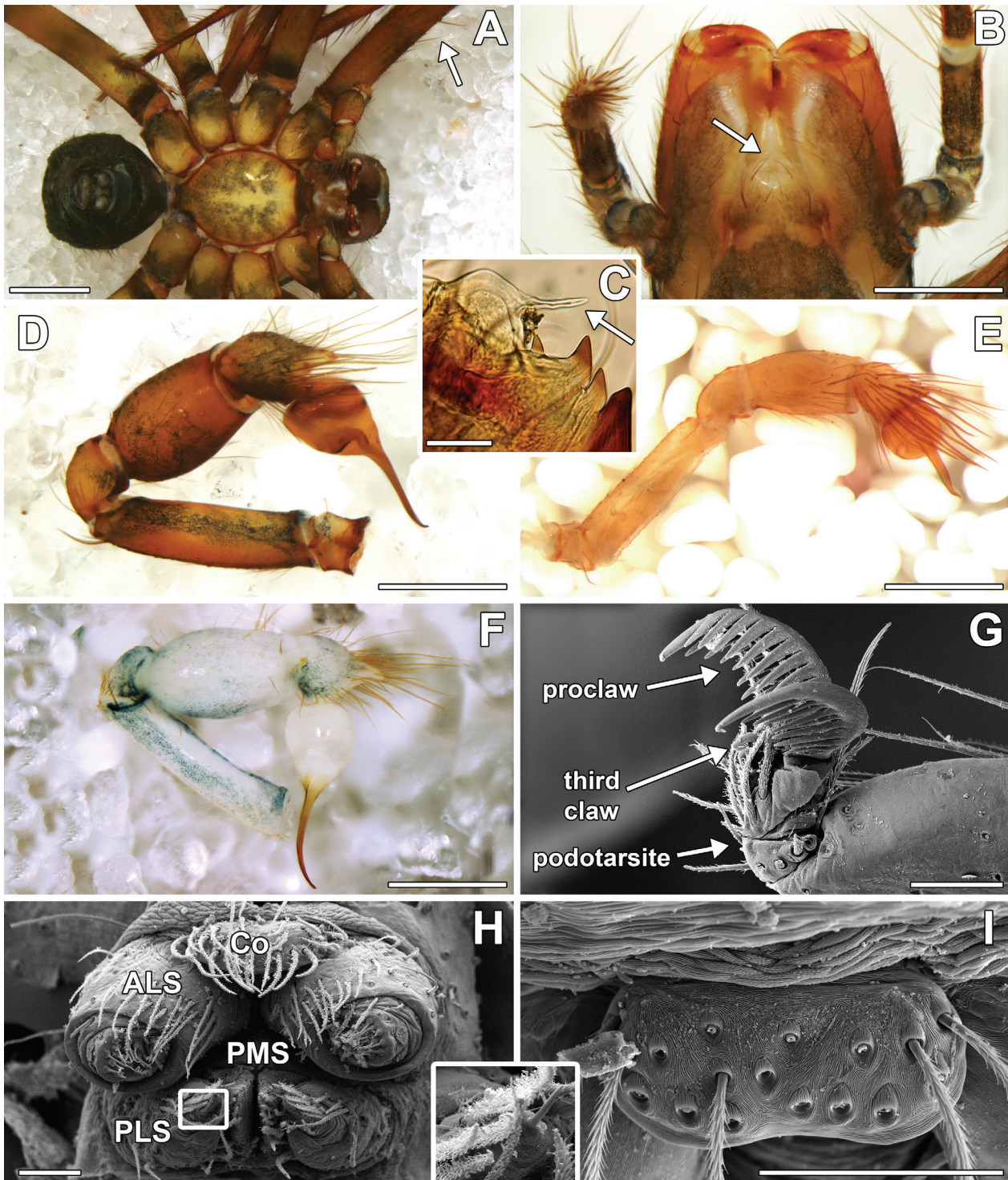


Figure 7. Extant drymusids from the Greater Antilles: *Drymusa spectata* Alayón (A, D) *Drymusa armasi* Alayón (B, C, F), and *Drymusa simoni* Bryant (E, G–I). A: male habitus, ventral (MNHNCu 51). Arrow to femoral macrosetae. B: female, mouthparts, ventral (MNHNCu 28). Arrow to notch in labium. C: female (MNHNCu 28), cheliceral lobe, arrow to distal prolongation. D: left palp, prolateral (MNHNCu 51). E: holotype male, left palp, prolateral (MCZ 23101). F: right palp, retrolateral (MNHNCu 28). G: immature paratype, left tarsal claws II, retrolateral (MCZ 44196). Notice double row of teeth in the proclaw. H: immature paratype, spinnerets, apical (MCZ 44196). Inset showing single spigot in the right posterior lateral spinneret. I: immature paratype, colulus, ventral (MCZ 44196). Scale bars: 1 mm (A), 0.5 mm (B, D–F), 0.05 mm (C, G–I).

two major ampullate gland spigots (Labarque et al. 2018: fig. 4C). *Drymusa* is supported by short, conical setae in the promarginal lobe of the chelicerae (see Labarque and Ramírez 2012) and the presence of a single acini-form gland spigot on the posterior lateral spinnerets (Fig.

7H). Finally, we recover a clade containing the extant *D. armasi* and *D. spectata* (both from the Antilles) and *L. aculicaput*, supported by three synapomorphies: the broad, plate-like colulus (Figs 5A, 7I), femoral macrosetae (Figs 3C, 7A) and the notched labium (Figs 4C, 7B).

3.3. Taxonomy

All three species are redescribed and re-diagnosed below. Based on the phylogenetic results, we propose the transfer of *Loxosceles aculicaput* from Sicariidae to *Drymusa* in Drymusidae, resulting in *Drymusa aculicaput* (Wunderlich, 2004) **comb. nov.** and new family assignment.

4. Discussion

4.1. Relationships among Scytodoidea families

The phylogenetic results we obtained are consistent with those of the most recent phylogeny with a broad sampling of Synspermiata families (Ramírez et al. 2021; ultra-conserved elements), although that study lacked Ochyroceratidae in its sampling. Our findings partially contradict the results found with morphology by Labarque and Ramírez (2012), who recovered Scytodidae (rather than Sicariidae) as closer to Periegopidae + Drymusidae; because our dataset includes a morphological matrix almost identical to Labarque and Ramírez's, it seems that the signal of the massive number of molecular markers (1912 markers) overrides that of morphological data (79 variant characters). Our results also contrast with those of Labarque et al. (2018; Sanger sequences) and Li et al. (2020; transcriptomes), who obtained Ochyroceratidae as sister to Scytodidae. It seems the phylogenetic position of ochyroceratids and psilodercids is far from settled (e.g., see the low bootstrap below *Althepus maechamensis* in the parsimony analysis, Fig. S5), although the evidence that they are indeed members of Scytodoidea is mounting. Discussing synapomorphies for the extended Scytodoidea (including Ochyroceratidae and Psilodercidae) is difficult since the morphology of both families needs further study. We recovered a single morphological synapomorphy for Scytodoidea (including Ochyroceratidae and Psilodercidae), the fused 3rd abdominal entapophyses. This might be an artifact of our taxon sampling, since some members of the Pholcoidea (the sister group of Scytodoidea) present this character state as well; also, it is open to interpretation, since the entapophyses are vestigial in Ochyroceratidae, Psilodercidae and Pholcoidea. The following node (Psilodercidae + the remaining Scytodoidea families) has a single synapomorphy: the simple (as opposed to branched) lateral tracheae in the posterior respiratory system.

4.2. Phylogenetic affinities of fossil species

We tested the position of *Loxosceles defecta* in the phylogeny of Scytodoidea and found it to be a true member of *Loxosceles*, supported in our analysis by the bifid cheliceral lamina (Fig. 1D). Other characters are also consistent with

this genus, such as the absence of a third tarsal claw (Fig. 1G). *Loxosceles* is divided into several species groups (see Gertsch 1967, Gertsch and Ennik 1983) and we strived to place the fossil into one of those groups by comparing its morphology to that of extant species (*L. simillima*, *L. hirsuta*, *L. laeta*, *L. rufescens*, *L. deserta*, *L. cubana*, and *L. caribbaea*, each belonging to a different clade; see Binford et al. 2008, Magalhaes et al. 2019). The cheliceral stridulatory files of *L. defecta* consist of relatively deep and well-delimited ridges (Fig. 1D) when compared to the shallow scales that had been documented for *L. rufescens* (see Labarque and Ramírez 2012: fig. 16E), and thus this was a potentially useful character. However, examination of several other *Loxosceles* revealed that deep ridges are the most common state in this genus, and only *L. rufescens* (among the species examined) presents shallow scales. Another potential synapomorphic state is the prolaterally expanded cymbium (Fig. 1I, arrow). Gertsch and Ennik (1983: 280) noted the “tarsus broadly lobed on the prolateral side” as diagnostic of the *L. reclusa* species group. Confirming this, we only observed this character state in *L. reclusa*, *L. cubana*, *L. taino*, *L. caribbaea* and *L. defecta*, suggesting it might be a synapomorphy of the *reclusa* group and indicating the fossil species belongs here (the prolateral shape of the cymbium is not observable in *L. deformis*, see Fig. 2D–F). Finally, *L. defecta* shows a few unusual features: the first tibia is sinuous, distally incrassate, and bears macrosetae (Fig. 1E–F). All *Loxosceles* species examined by us have straight tibiae; only *Loxosceles laeta* has a sinuous first metatarsus with strong setae. The only known species with a sinuous tibia is *L. carinhanha* Bertani, von Schimonsky et Gallão, 2018, from Brazil (see Bertani et al. 2018: fig. 34), but it apparently belongs to the distantly related *amazonica* group, although its phylogenetic position remains untested. Thus, it might be that this character state evolved independently in *L. carinhanha* and *L. defecta*. Regarding the strong macrosetae, the only species examined by us whose tibia bears strong macrosetae is *L. cubana* (Fig. 8). *Loxosceles caribbaea* and *L. taino* (examined by us) and other members of the *reclusa* group from the mainland (A. Valdez-Mondragón, pers. comm.) lack such tibial macrosetae, although a few species present strong macrosetae in the first femur. Thus, the strong macrosetae in the tibia may be a synapomorphy uniting *L. defecta* with *L. cubana*, and indicate the fossil could be more closely related to the Antillean species of the *reclusa* species group.

We could not include *Loxosceles deformis* in the phylogeny, since the only known individual is poorly preserved and details of the legs, chelicerae, and spinnerets cannot be observed. However, the genitalia is similar to that of *L. defecta*, and it has the flattened, ribbon-shaped embolus that is common in the *Loxosceles reclusa* species group (see Gertsch and Ennik 1983). It also lacks the third claw and has an elongate palpal femur that is synapomorphic of *Loxosceles* (see Magalhaes et al. 2017a). Thus, we conclude that it is a true member of the genus, most likely in the *Loxosceles reclusa* species group.

We here transfer *Loxosceles aculicaput* to *Drymusa*. This species presents three tarsal claws (Fig. 3F),

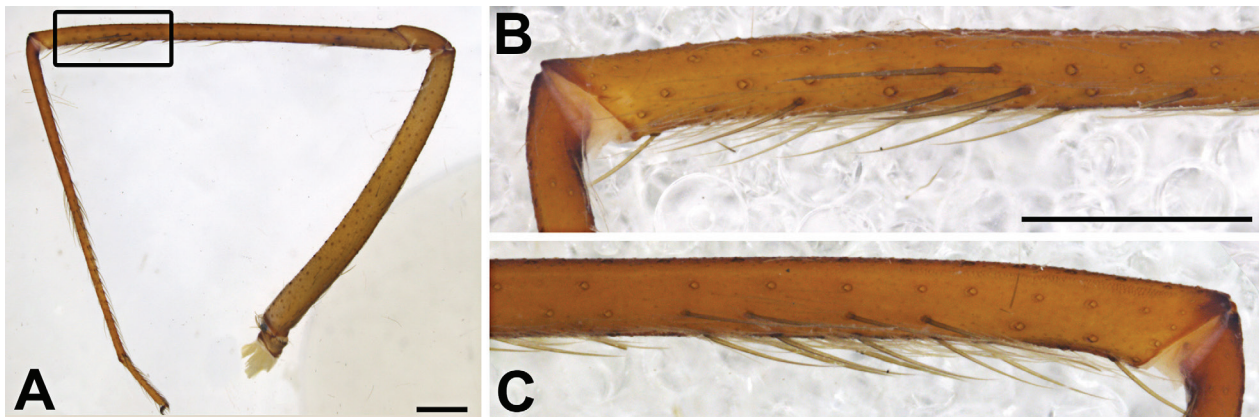


Figure 8. *Loxosceles cubana* Gertsch, male (IBSP 164702), left leg I. Inset in A marking area with retrolateral macrosetae on the tibia. **A, B** Retrolateral view. **C** Prolateral view. Scale bars: 1 mm.

a well-developed podotarsite (Fig. 3F), relatively short anterior lateral spinnerets (Fig. 3D), and the spinnerets are in a compact group (Fig. 4B). All of these characters dispute a placement in *Loxosceles*, which presents only two tarsal claws in a poorly developed podotarsite (Labarque and Ramírez 2012: fig. 5A, B), relatively long anterior spinnerets, and a diastema between the anterior and posterior spinnerets (Magalhaes et al. 2017b: fig. 1). Our phylogenetic results (Fig. 6) suggest a placement in *Drymusa* instead, particularly close to extant Antillean species, based on three characters: the broad colulus (Figs 5A, 7I), the femoral macrosetae (Figs 3C, 7A) and the notched labium (Figs 4C, 7B). Interestingly, two of these characters were revealed by imaging the piece with SR μ CT, highlighting the usefulness of this technique in the study of fossils. The genitalia of *Drymusa aculicaput* **comb. nov.** are here studied in detail for the first time (Fig. 5D–J). They are similar to other species of *Drymusa*, including the Antillean representatives, in the short, incrassate tibia and the cymbium with a small apical extension (see Fig. 7D–F), but are clearly different from the extant Hispaniolan species *Drymusa simoni* (see 5.2.1).

4.3. Biogeographic implications

Penney (1999) observed that extant, endemic species of *Drymusa* can be found today in Hispaniola and that fossils would shed light on the timing of arrival of this group to the islands. The discovery that *Drymusa aculicaput* **comb. nov.** belongs in this genus indicates the genus arrived at Hispaniola during (or before) the Miocene. It is also a crown *Drymusa*, showing the genus had diversified by this epoch, and thus that it is an ancient group. It is not unlikely that the separation between the African *Izithunzi* and the American *Drymusa* pre-dates the separation of these continents, as is the case of *Sicarius* and *Loxosceles* (Binford et al. 2008; Magalhaes et al. 2019). A more complete phylogeny of drymusids, building on previous efforts by Labarque et al. (2018), will be useful to put this hypothesis to test, and will certainly benefit from the new morphological data on *D. aculicaput* **comb. nov.** gathered here.

4.4. Conclusions

Our phylogenetic and taxonomic revision of spider taxa preserved in Dominican amber and previously assigned to *Loxosceles* allows us to conclude:

- (1) *Loxosceles defecta* and *L. deformis* are *bona fide* members of this genus, and *L. defecta* can be further placed in the *L. reclusa* species group based on the prolaterally expanded palpal cymbium; this species also presents an incrassate first tibia bearing macrosetae. Tibial macrosetae are also present in the extant species *Loxosceles cubana*, suggesting that *L. defecta* may be closely related to extant taxa from the Antilles.
- (2) *Loxosceles aculicaput* presents three claws and shares a broad colulus, femoral macrosetae, and a notched labium with extant members of *Drymusa* inhabiting the Antilles, and thus was misplaced in *Loxosceles*; we here propose the **new combination** *Drymusa aculicaput*, representing the first known fossil of Drymusidae. This extends the stratigraphic range of crown *Drymusa* to the Miocene and indicates these spiders had already reached the islands by then.

5. Taxonomy

5.1. Genus *Loxosceles* Heineken et Lowe, 1832 [Family Sicariidae Keyserling, 1880]

Type species. *Loxosceles citigrada* Heineken et Lowe [junior synonym of *Loxosceles rufescens* (Dufour)] (extant, Mediterranean region to Middle East).

5.1.1. *Loxosceles defecta* Wunderlich, 1988

Fig. 1

Loxosceles defecta Wunderlich, 1988: 69, figs 92–94.

Type material. Adult male holotype and adult male paratype in the same Dominican amber piece, holotype SMF Be 970a, paratype SMF Be 970b, deposited in SMF, examined. No other specimens are known.

Preservation. Both spiders are preserved in the same reddish yellow amber piece. Both individuals are partly incomplete and preserved in moderate condition. In both spiders the abdomen is severely shrunk. The holotype has both palps (right palp slightly deformed, with a bubble trapped in the tibia), while the paratype has none. The holotype is missing right leg I, right leg IV and parts of right legs II and III; left leg I is detached from the body and preserved to the left of the animal. The paratype has all the legs on the right side but they are distinctly deformed and covered by emulsion; only part of femur IV remains in the left side. Syninclusions: a large leg of an entelegyne spider, a leaf, and a Collembola.

Diagnosis. *Loxosceles defecta* can be diagnosed from the other *Loxosceles* in Dominican amber (*L. deformis*), as well as from extant Antillean species, by the sinuous, distally incrassate first tibia bearing macrosetae (Fig. 1E, F); the palp has a gently curved, flattened embolus that is ~1.5 times as long as the globose base of the bulb and is less flattened than that of *L. deformis*.

Description. Male holotype (SMF-Be 970a). **Structure:** Carapace slightly wider than long, narrowed anteriorly, particularly hirsute in the cephalic region, with a well-developed fovea. Leg I with sinuous tibia, distally incrassate, with ~5 visible macrosetae in the retrolateral face of the incrassate portion (Fig. 1E); third claw absent. Palps (Fig. 1H, I); femur elongate; tibia slightly incrassate, ventrally bulging; cymbium short and blunt, prolaterally bulging; bulb with small globose base and gently curved, flattened, slightly sinuous embolus. **Measurements** [mm]: Total length not possible to measure. Carapace length 1.98, width 2.02. Abdomen damaged. Palpal femur length 1.13. Palpal tibia length 0.70, height 0.35. Leg I: femur 3.08, patella 0.74, tibia 4.44, metatarsus and tarsus not possible to measure. Leg II: femur 3.37, patella 0.79, tibia 4.40, not possible to measure from metatarsus. Leg III: femur 2.23, not possible to measure from patella. Leg IV: femur 6.34, patella 1.64, tibia 3.76, metatarsus and tarsus damaged. — Male paratype (SMF-Be 970b). **Structure:** Six eyes in three dyads separated by 1–2 eye diameters (Fig. 2C). Chelicerae with stridulatory files formed by deep ridges (Fig. 2D), bifid cheliceral lamina and large promarginal lobe; teeth absent. Tibia I deformed, distally incrassate bearing macrosetae.

5.1.2. *Loxosceles deformis* Wunderlich, 1988

Fig. 2

Loxosceles deformis Wunderlich, 1988: 68, fig. 90.

Type material. Holotype adult male in Dominican amber, SMF Be 968a, deposited in SMF, examined. No other specimens are known.

Preservation. The spider is incompletely preserved in a reddish yellow piece of amber. The abdomen is severely shriveled. The anterior portion of the prosoma is covered by emulsion. Only left legs I and III and right femur II are preserved. The left palp, as well as the right palpal tibia, are strongly deformed. Syninclusions: two small Lepidoptera, a nematoceran Diptera, an Acari, a Hymenoptera: Formicidae, another unidentified spider with fungi, and a Bryophyta.

Diagnosis. *Loxosceles deformis* can be diagnosed from the *Loxosceles* in Dominican amber (*L. defecta*) by the unmodified first tibia (Fig. 2C); the palp has a gently curved, flattened embolus that is twice as long as the globose base of the bulb. Among extant Antillean species, it is most similar to *L. caribbaea* (see Sánchez-Ruiz and Brescovit: 2013: figs 1, 2) but can be distinguished by the longer, more flattened embolus.

Description. Male holotype (SMF-Be 968a). **Structure:** Carapace almost as wide as long, narrowed anteriorly, particularly hirsute in the cephalic region. Six eyes in three dyads. Legs without strong macrosetae; tibia I unmodified; tarsus III with only two claws. Details of mouthpieces and spinnerets not visible. Palp (Fig. 2D–F): palpal femur as long as patella + tibia; tibia slightly incrassate, bulging ventrally, distally deformed; cymbium small, blunt, bulging dorsally; bulb with small globose base and long, flattened, gently curved embolus. **Measurements** [mm]: Total length (excluding chelicerae and spinnerets) 6.09. Carapace length 3.00, width 2.97. Abdomen length 3.43, width 1.80. Palpal femur length 1.59. Palpal tibia length 0.83, height 0.40. Leg I: femur 4.80, patella 1.07, tibia 5.60, metatarsus 4.22, tarsus 1.12. Leg II: femur 4.93, missing from patella. Leg III: femur 4.93, patella 1.12, tibia 4.85, metatarsus 4.81, tarsus 0.68. Leg IV missing.

5.2. Genus *Drymusa* Simon, 1892 [Family Drymusidae Simon, 1893]

Type species. *Drymusa nubila* Simon (extant, Saint Vincent).

5.2.1. *Drymusa aculicaput* (Wunderlich, 2004) new combination

Figs 3–5

Loxosceles aculicaput Wunderlich, 2004: 703, fig. 10b–d, photo 36.

Type material. Holotype adult male in Dominican amber, deposited in SMNG 07/36287-422, labeled F933/

DB/AR/LOX/CJW, examined. No other specimens are known.

Preservation. The spider is completely and well-preserved in an orange piece of amber. The abdomen is slightly shrunken and shriveled but no other structures are obviously deformed. The amber piece has large fissures in the portion ventral to the spider. The piece has been embedded in artificial resin. There are no syninclusions other than some pieces of unidentifiable plants and detritus.

Diagnosis. *Drymusa aculicaput* **comb. nov.** can be distinguished from other scytodoids preserved in Dominican amber, as well as from extant congeners, by the palp with short, incrassate tibia and by the bulb with a thin, straight, needle-like embolus (Fig. 5E, G, H, J).

Description. Male holotype (SMNG 07/36287-422).

Structure: Carapace longer than wide, narrowed and more hirsute in the cephalic region. Six eyes in three dyads separated by 2–3 diameters (Fig. 4D). Chelicera with basal article robust (Figs 3G, 4D); cheliceral lamina present, with broad, triangular apex; at least one promarginal tooth present. Endites not converging in front of labium; anterior margin of labium notched (Fig. 4C). Sternum slightly longer than wider. Legs long and thin (Figs 3A, 4A) with a few macrosetae on the prolateral face of the first femur (Fig. 3C) and on the ventral faces of all tibiae and metatarsi. Well-developed podotarsite; third claw present (Fig. 3F). Spinnerets in a compact group (Fig. 5B); colulus broad (Fig. 5A); ALS short and broad, barely longer than PLS (Figs 4D, 5C). Palps (Fig. 5D–J): tibia shorter than femur, incrassate; cymbium short with a small apical extension; bulb with globose, rounded base and thin, straight, needle-shaped embolus. — **Measurements** [mm]: Total length (excluding chelicerae and spinnerets) 2.34. Carapace length 1.15, width 0.89. Abdomen length 1.27, width 0.66. Palpal femur length 0.52. Palpal tibia length 0.24, height 0.21. Leg I: femur 2.87, patella 0.27, tibia 3.05, metatarsus 0.91, tarsus 2.25. Leg II: femur 2.74, patella 0.38, tibia 2.67, metatarsus 3.65, tarsus 0.66. Leg III: femur 2.13, patella 0.27, tibia 1.88, metatarsus 1.95, tarsus 0.72. Leg IV: femur 2.58, patella 0.33, tibia 2.67, metatarsus 2.55, tarsus 0.72.

6. Competing interests

The authors have declared that no competing interests exist.

7. Acknowledgements

We are indebted to curators and curatorial staff from the collections holding the material studied in this revision. We thank Alejandro Valdez Mondragón for sharing information on the morphology of members of the *Loxosceles reclusa* species group, Solanlly Carrero for sharing information on extant *Drymusa* from the Dominican Republic, and the late Norman Platnick for organizing a collecting expedition with APG

in Cuba. We thank Guilherme Azevedo and Rodrigo Monjaraz-Ruedas, from San Diego State University, for help with processing genomic data. Earlier versions of the text benefited from comments by Michael Rix, Charles Griswold and the editors, Lorenzo Prendini and Klaus Klass. This research received support from the SYNTHESYS+ Project www.synthesys.info, which is financed by the European Commission via the H2020 Research Infrastructure programme (grant DE-TAF-1356 to ILFM). ILFM was supported by a CONICET postdoctoral fellowship. This study was financially supported by Fondo para la Investigación Científica y Tecnológica (PICT 2015-0283, PICT 2017-2689, PICT-2019-2745), Consejo Nacional de Investigaciones Científicas y Técnicas (PUE 098), and the German VolkswagenStiftung [Project N. 90946]. We acknowledge DESY (Hamburg, Germany), a member of the Helmholtz Association HGF, for the provision of experimental facilities. Parts of this research were carried out at PETRA III [BAG-20190010].

8. References

- Azevedo GHF, Parreiras JS, Bougie T, Michalik P, Wunderlich J, Ramirez MJ (2021) Fossils constrain biogeographical history in a clade of flattened spiders with transcontinental distribution. *Journal of Biogeography* 48: 3032–3046. [www.doi.org/10.1111/jbi.14259](https://doi.org/10.1111/jbi.14259)
- Bertani R, von Schimonsky DM, Gallão JE, Bichuette ME (2018) Four new troglomorphic species of *Loxosceles* Heineken & Lowe, 1832: contributions to the knowledge of recluse spiders from Brazilian caves (Araneae, Sicariidae). *ZooKeys* 806: 47–72. [www.doi.org/10.3897/zookeys.806.27404](https://doi.org/10.3897/zookeys.806.27404)
- Binford GJ, Callahan MS, Bodner MR, Rynerson MR, Núñez PB, Ellison CE, Duncan RP (2008) Phylogenetic relationships of *Loxosceles* and *Sicarius* spiders are consistent with Western Gondwanan vicariance. *Molecular Phylogenetics and Evolution* 49: 538–53. [www.doi.org/10.1016/j.ympev.2008.08.003](https://doi.org/10.1016/j.ympev.2008.08.003)
- Bolger AM, Lohse M, Usadel B (2014) Trimmomatic: A flexible trimmer for Illumina Sequence Data. *Bioinformatics*, btu170. [www.doi.org/10.1093/bioinformatics/btu170](https://doi.org/10.1093/bioinformatics/btu170)
- Brescovit AD, Ruiz AS, Alayón-García G (2016) The Filistatidae in the Caribbean region, with a description of the new genus *Antilloides*, revision of the genus *Filistatoides* F. O. P.-Cambridge and notes on *Kukulcania* Lehtinen (Arachnida, Araneae). *Zootaxa* 4136: 401–432. [www.doi.org/10.11646/zootaxa.4136.3.1](https://doi.org/10.11646/zootaxa.4136.3.1)
- Castresana J (2000) Selection of conserved blocks from multiple alignments for their use in phylogenetic analysis. *Molecular Biology and Evolution* 17: 540–552. [www.doi.org/10.1093/oxfordjournals.molbev.a026334](https://doi.org/10.1093/oxfordjournals.molbev.a026334)
- Dunlop JA, Penney D, Dalüge N, Jäger P, McNeil A, Bradley RS, Withers PJ, Preziosi RF (2011) Computed tomography recovers data from historical amber: an example from huntsman spiders. *Naturwissenschaften* 98: 519–527. [www.doi.org/10.1007/s00114-011-0796-x](https://doi.org/10.1007/s00114-011-0796-x)
- Dunlop JA, Penney D, Jekel D (2020) A summary list of fossil spiders and their relatives. In: *World Spider Catalog*. Natural History Museum Bern, online at <http://wsc.nmbe.ch>, version 20.5, accessed on 11/01/2022.
- Faircloth BC (2016) PHYLUCES is a software package for the analysis of conserved genomic loci. *Bioinformatics* 32: 786–788. [www.doi.org/10.1093/bioinformatics/btv646](https://doi.org/10.1093/bioinformatics/btv646)
- Fu L, Niu B, Zhu Z, Wu S, Li W (2012) CD-HIT: accelerated for clustering the next-generation sequencing data. *Bioinformatics* 28: 3150–3152. [www.doi.org/10.1093/bioinformatics/bts565](https://doi.org/10.1093/bioinformatics/bts565)

- Gertsch WJ (1967) The spider genus *Loxosceles* in South America. Bulletin of American Museum of Natural History 136: 121–182.
- Gertsch WJ, Ennik F (1983) The spider genus *Loxosceles* in North America, Central America, and the West Indies (Araneae, Loxoscelidae). Bulletin of the American Museum of Natural History 175: 264–360.
- Goloboff PA, Catalano SA (2016) TNT version 1.5, including a full implementation of phylogenetic morphometrics. Cladistics 32: 221–238. www.doi.org/10.1111/cla.12160
- Greving I, Wilde F, Ogurreck M, Herzen J, Hammel JU, Hipp A, Friedrich F, Lottermoser L, Dose T, Burmester H, Müller M, Beckmann F (2014) P05 imaging beamline at PETRA III: first results. Proceedings of SPIE Developments in X-Ray Tomography IX, 9212: 1–9.
- Griswold CE, Ramirez MJ, Coddington JA, Platnick NI (2005) Atlas of phylogenetic data for entelegyne spiders (Araneae: Araneomorphae: Entelegynae) with comments on their phylogeny. Proceedings of the California Academy of Sciences 56: 1–324.
- Hoang DT, Chernomor O, von Haeseler A, Minh BQ, Vinh LS (2018) UFBoot2: Improving the ultrafast bootstrap approximation. Molecular Biology and Evolution 35: 518–522. www.doi.org/10.1093/molbev/msx281
- Kalyaanamoorthy S, Minh BQ, Wong TKF, von Haeseler A, Jermiin LS (2017) ModelFinder: Fast model selection for accurate phylogenetic estimates. Nature Methods 14: 587–589. www.doi.org/10.1038/nmeth.4285
- Katoh K, Rozewicki J, Yamada KD (2017) MAFFT online service: multiple sequence alignment, interactive sequence choice and visualization. Briefings in Bioinformatics 30: 3059. www.doi.org/10.1093/bib/bbx108
- Kulkarni S, Wood H, Lloyd M, Hormiga G (2020) Spider-specific probe set for ultraconserved elements offers new perspectives on the evolutionary history of spiders (Arachnida, Araneae). Molecular Ecology Resources 20: 185–203. www.doi.org/10.1111/1755-0998.13099
- Labarque FM, Ramirez MJ (2012) The placement of the spider genus *Periegops* and the phylogeny of Scytodoidea (Araneae: Araneomorphae). Zootaxa 3312: 1–44. www.doi.org/10.11646/zootaxa.3312.1.1
- Labarque FM, Wolff JO, Michalik P, Griswold CE, Ramirez MJ (2017) The evolution and function of spider feet (Araneae: Arachnida): multiple acquisitions of distal articulations. Zoological Journal of the Linnean Society 181: 308–341. www.doi.org/10.1093/zoolinnean/zlw030
- Labarque FM, Pérez-González A, Griswold CE (2018) Molecular phylogeny and revision of the false violin spiders (Araneae: Drymusidae) of Africa. Zoological Journal of the Linnean Society 183: 390–430. www.doi.org/10.1093/zoolinnean/zlx088
- Li F, Shao L, Li S (2020) Tropical niche conservatism explains the Eocene migration from India to Southeast Asia in ochyroceratid spiders. Systematic Biology 69: 987–998. www.doi.org/10.1093/sysbio/syaa006
- Magalhaes ILF, Ramirez MJ (2022) Phylogeny and biogeography of the ancient spider family Filistatidae (Araneae) is consistent both with long-distance dispersal and vicariance following continental drift. Cladistics 38: 538–562. www.doi.org/10.1111/cla.12505
- Magalhaes ILF, Brescovit AD, Santos AJ (2017a) Phylogeny of Sicariidae spiders (Araneae: Haplogynae), with a monograph on Neotropical *Sicarius*. Zoological Journal of the Linnean Society 179: 767–864. www.doi.org/10.1111/zoj.12442
- Magalhaes ILF, Ravelo AM, Scioscia CL, Peretti AV, Michalik P, Ramirez MJ (2017b) Recluse spiders produce flattened silk rapidly using a highly modified, self-sufficient spinning apparatus. Journal of Zoology 303: 27–35. www.doi.org/10.1111/jzo.12462
- Magalhaes ILF, Neves DM, Santos FR, Vidigal THDA, Brescovit AD, Santos AJ (2019) Phylogeny of Neotropical *Sicarius* sand spiders suggests frequent transitions from deserts to dry forests despite antique, broad-scale niche conservatism. Molecular Phylogenetics and Evolution 140: 106569. www.doi.org/10.1016/j.ympev.2019.106569
- Magalhaes ILF, Azevedo GHF, Michalik P, Ramirez MJ (2020) The fossil record of spiders revisited: implications for calibrating trees and evidence for a major faunal turnover since the Mesozoic. Biological Reviews 95: 184–217. www.doi.org/10.1111/brv.12559
- Minh BQ, Schmidt HA, Chernomor O, Schrempf D, Woodhams MD, von Haeseler A, Lanfear R (2020) IQ-TREE 2: New models and efficient methods for phylogenetic inference in the genomic era. Molecular Biology and Evolution 37: 1530–1534. www.doi.org/10.1093/molbev/msaa015
- Mongiardino Koch N, Thompson JR (2021) A total-evidence dated phylogeny of Echinoidea combining phylogenomic and paleontological data. Systematic Biology 70: 421–439. www.doi.org/10.1093/sysbio/syaa069
- Moosmann J, Ershov A, Weinhardt V, Baumbach T, Prasadet MS, Labonne C, Xiao X, Kashef J, Hofmann R (2014) Time-lapse X-ray phase-contrast microtomography for in vivo imaging and analysis of morphogenesis. Nature Protocols 9: 294–304.
- Nyffeler M, Birkhofer K (2017) An estimated 400–800 million tons of prey are annually killed by the global spider community. Science of Nature 104: 30. www.doi.org/10.1007/s00114-017-1440-1
- Palenstijn WJ, Batenburg KJ, Sijbers J (2011) Performance improvements for iterative electron tomography reconstruction using graphics processing units (GPUs). Journal of Structural Biology 176(2): 250–253.
- Pérez-González A, Rubio GD, Ramirez MJ (2016) Insights on vulval morphology in Ochyroceratinae with a rediagnosis of the subfamily and description of the first Argentinean species (Araneae: Synspermiata: Ochyroceratidae). Zoologischer Anzeiger 260: 33–44. www.doi.org/10.1016/j.jcz.2015.12.001
- Planas E, Ribera C (2014) Uncovering overlooked island diversity: colonization and diversification of the medically important spider genus *Loxosceles* (Arachnida: Sicariidae) on the Canary Islands. Journal of Biogeography 41: 1255–1266.
- Penney D (1999) Hypotheses for the recent Hispaniolan spider fauna based on the Dominican Republic Amber spider fauna. Journal of Arachnology 27: 64–70.
- Penney D (2005) First fossil Filistatidae: a new species of *Misionella* in Miocene amber from the Dominican Republic. Journal of Arachnology 33: 93–100.
- Penney D, Pérez-Gelabert DE (2002) Comparison of the Recent and Miocene Hispaniolan spider faunas. Revista Ibérica de Aracnología 6: 203–223.
- Penney D, Dierick M, Cnudde V, Masschaele B, Vlassenbroeck J, Van Hoorebeke L, Jacobs P (2007) First fossil Micropholcommatidae (Araneae), imaged in Eocene Paris amber using X-Ray computed tomography. Zootaxa 1623: 47–53. www.doi.org/10.11646/zootaxa.1623.1.3
- Penney D, McNeil A, David DI, Bradley R, Withers PJ, Preziosi RF (2012) The oldest fossil pirate spider (Araneae: Mimetidae), in uppermost Eocene Indian amber, imaged using X-ray computed tomography. Bulletin of the British Arachnological Society 15: 299–302. www.doi.org/10.13156/arak.2012.15.9.299

- Prijbelski A, Antipov D, Meleshko D, Lapidus A, Korobeynikov A (2020) Using SPAdes de novo assembler. *Current Protocols in Bioinformatics* 70(1): e102. www.doi.org/10.1002/cpbi.102
- Ramírez MJ (2014) The morphology and phylogeny of dionychan spiders (Araneae, Araneomorphae). *Bulletin of the American Museum of Natural History* 390: 1–375. www.doi.org/10.1206/821.1
- Ramírez MJ, Magalhaes ILF, Derkarabetian S, Ledford J, Griswold CE, Wood HM, Hedin M (2021) Sequence capture phylogenomics of true spiders reveals convergent evolution of respiratory systems. *Systematic Biology* 70: 14–20. www.doi.org/10.1093/sysbio/syaa043
- Sadowski E-M, Schmidt AR, Seyfullah LJ, Solórzano-Kraemer MM, Neumann C, Perrichot V, Hamann C, Milke R, Nascimbene PC (2021) Conservation, preparation and imaging of diverse ambers and their inclusions. *Earth-Science Reviews* 220: 103653.
- Saupe EE, Pérez-de la Fuente R, Selden PA, Delclòs X, Tafforeau P, Soriano C (2012) New *Orchestina* Simon, 1882 (Araneae: Oonopidae) from Cretaceous ambers of Spain and France: first spiders described using phase-contrast X-ray synchrotron microtomography. *Palaeontology* 55: 127–143. www.doi.org/10.1111/j.1475-4983.2011.01123.x
- Sánchez-Ruiz A, Brescovit AD (2013) The genus *Loxosceles* Heineken & Lowe (Araneae: Sicariidae) in Cuba and Hispaniola, West Indies. *Zootaxa* 3731: 212–222. www.doi.org/10.11646/zootaxa.3731.2.2
- Selden PA, Penney D (2010) Fossil spiders. *Biological Reviews* 85: 171–206. www.doi.org/10.1111/j.1469-185X.2009.00099.x
- Solórzano Kraemer MM, Perrichot V, Brown B, Soriano C, Tafforeau P (2011) A new species of the Cretaceous genus *Prioriphora* (Diptera: Phoromorpha) in France amber. *Systematic Entomology* 36: 581–588. www.doi.org/10.1111/j.1365-3113.2011.00583.x
- Solórzano Kraemer MM, Perrichot V, Soriano C, Damgaard J (2014) Fossil water striders in Cretaceous French amber (Heteroptera: Gerromorpha: Mesoveliidae and Veliidae). *Systematic Entomology* 39(3): 590–605. www.doi.org/10.1111/syen.12077
- Solórzano Kraemer MM, Delclòs X, Clapham ME, Arillo A, Peris D, Jäger P, Stebner F, Peñalver E (2018) Arthropods in modern resins reveal if amber accurately recorded forest arthropod communities. *Proceedings of the National Academy of Sciences of the United States of America* 115: 6739–6744. www.doi.org/10.1073/pnas.1802138115
- Solórzano-Kraemer MM, Delclòs X, Engel MS, Peñalver E (2020) A revised definition for copal and its significance for palaeontological and Anthropocene biodiversity-loss studies. *Scientific Reports* 10: 1–12.
- Solórzano-Kraemer MM, Kunz R, Hammel JÜ, Peñalver E, Delclòs X, Engel MS (in press) Stingless bees (Hymenoptera: Apidae) in Holocene copal and Defaunation resin from Eastern Africa indicate Recent biodiversity change. *The Holocene* 32(5): 414–432. www.doi.org/10.1177/09596836221074035
- Soriano C, Archer M, Azar D, Creaser Ph, Delclòs X, Godthelp H, Hand S, Jones A, Nel A, Néraudeau D, Ortega-Blanco J, Pérez-de la Fuente R, Perrichot V, Saupe E, Solórzano Kraemer MM, Tafforeau P (2010) Synchrotron X ray imaging of inclusions in amber. *Comptes Rendus Palevol* 9: 361–368. www.doi.org/10.1016/j.crpv.2010.07.014
- Starrett J, Derkarabetian S, Hedin M, Bryson Jr RW, McCormack JE, Faircloth BC (2017) High phylogenetic utility of an ultraconserved element probe set designed for Arachnida. *Molecular Ecology Resources* 17: 812–823. www.doi.org/10.1111/1755-0998.12621
- Vetter RS (2008) Spiders of the genus *Loxosceles* (Araneae, Sicariidae): a review of biological, medical and psychological aspects regarding envenomations. *Journal of Arachnology* 36: 150–163. www.doi.org/10.1636/RSt08-06.1
- van Aarle W, Palenstijn WJ, Cant J, Janssens E, Bleichrodt F, Dabravolski A, De Beenhouwer J, Batenburg J, Sijbers J (2016) Fast and flexible X-ray tomography using the ASTRA toolbox. *Optics Express* 24(22): 25129–25147.
- van Aarle W, Palenstijn WJ, De Beenhouwer J, Altantzis T, Bals S, Batenburg KJ, Sijbers J (2015) The ASTRA Toolbox: A platform for advanced algorithm development in electron tomography. *Ultramicroscopy* 157: 35–47.
- Wilde F, Ogurreck M, Greving I, Schreyer A (2016) Micro-CT at the imaging beamline P05 at PETRA III. *AIP Conference Proceedings* 1741(1): 030035.
- Wood HM (2017) Integrating fossil and extant lineages: an examination of morphological space through time (Araneae: Archaeidae). *Journal of Arachnology* 45: 20–29. www.doi.org/10.1636/JoA-S-16-039.1
- Wood HM, Matzke NJ, Gillespie RG, Griswold CE (2013) Treating fossils as terminal taxa in divergence time estimation reveals ancient vicariance patterns in the palpimanoid spiders. *Systematic Biology* 62: 264–284. www.doi.org/10.1093/sysbio/sys092
- WSC (2022). World Spider Catalog. Version 22.5. Natural History Museum Bern, online at <http://wsc.nmbe.ch>, accessed on 11/01/2022. www.doi.org/10.24436/2
- Wunderlich J (1986) *Spinnenfauna Gestern und Heute. Fossile Spinnen in Bernstein und ihre heute lebenden Verwandten*. Erich Bauer Verlag bei Quelle und Meyer, Wiesbaden, 283 pp.
- Wunderlich J (1988) Die fossilen Spinnen im Dominikanischen Bernstein. *Beiträge zur Araneologie* 2: 1–378.
- Wunderlich J (2004) Fossil spiders (Araneae) of the superfamily Dysderoidea in Baltic and Dominican amber, with revised family diagnoses. *Beiträge zur Araneologie* 3: 633–746.

Supplementary material 1

Figures S1–S5

Authors: Magalhaes ILF, Pérez-González A, Labarque FM, Carboni M, Hammel JU, Kunz R, Ramírez MJ, Solórzano-Kraemer MM (2022)

Data type: .pdf

Explanation note: **Fig. S1.** Maximum likelihood tree estimated from target-gene molecular markers. — **Fig. S2.** Maximum likelihood tree estimated from ultraconserved elements. — **Fig. S3.** Maximum likelihood and maximum parsimony trees estimated from sequence data (target genes + ultraconserved elements). — **Fig. S4.** Maximum likelihood and maximum parsimony trees estimated from morphology. — **Fig. S5.** Maximum likelihood and maximum parsimony trees estimated from the total evidence dataset.

Copyright notice: This dataset is made available under the Open Database License (<http://opendatacommons.org/licenses/odbl/1.0>). The Open Database License (ODbL) is a license agreement intended to allow users to freely share, modify, and use this Dataset while maintaining this same freedom for others, provided that the original source and author(s) are credited.

Link: <https://doi.org/asp.80.e86008.suppl1>

Supplementary material 2

Morphological matrix

Authors: Magalhaes ILF, Pérez-González A, Labarque FM, Carboni M, Hammel JU, Kunz R, Ramírez MJ, Solórzano-Kraemer MM (2022)

Data type: .tnt

Explanation note: Morphological matrix in TNT format (<http://www.lillo.org.ar/phylogeny/tnt>).

Copyright notice: This dataset is made available under the Open Database License (<http://opendatacommons.org/licenses/odbl/1.0>). The Open Database License (ODbL) is a license agreement intended to allow users to freely share, modify, and use this Dataset while maintaining this same freedom for others, provided that the original source and author(s) are credited.

Link: <https://doi.org/asp.80.e86008.suppl2>

Supplementary material 3

DNA alignments and partition file

Authors: Magalhaes ILF, Pérez-González A, Labarque FM, Carboni M, Hammel JU, Kunz R, Ramírez MJ, Solórzano-Kraemer MM (2022)

Data type: .zip

Explanation note: DNA alignments and partition file for the maximum likelihood analysis.

Copyright notice: This dataset is made available under the Open Database License (<http://opendatacommons.org/licenses/odbl/1.0>). The Open Database License (ODbL) is a license agreement intended to allow users to freely share, modify, and use this Dataset while maintaining this same freedom for others, provided that the original source and author(s) are credited.

Link: <https://doi.org/asp.80.e86008.suppl3>

Supplementary material 4

Tree from the total evidence analysis

Authors: Magalhaes ILF, Pérez-González A, Labarque FM, Carboni M, Hammel JU, Kunz R, Ramírez MJ, Solórzano-Kraemer MM (2022)

Data type: .nwk

Explanation note: Tree from the total evidence, maximum likelihood analysis in Newick format.

Copyright notice: This dataset is made available under the Open Database License (<http://opendatacommons.org/licenses/odbl/1.0>). The Open Database License (ODbL) is a license agreement intended to allow users to freely share, modify, and use this Dataset while maintaining this same freedom for others, provided that the original source and author(s) are credited.

Link: <https://doi.org/asp.80.e86008.suppl4>